Climate Dynamics (2022) 59:1297–1307
https://doi.org/10.1007/s00382-021-06038-7

Increased occurrence of day–night hot extremes in a warming climate

Jinxin Zhu[1] · Shuo Wang[2] · Erich Markus Fischer[3]

Received: 21 May 2021 / Accepted: 3 November 2021 / Published online: 15 November 2021

Abstract

Climate change leads to a more frequent occurrence of hot days (HDs) and hot nights (HNs). The consecutive occurrence of HDs and HNs (COHs) is often used as a measure of the persistence of an extremely hot spell. Nonetheless, the combined effect of air temperature and relative humidity on the changing COHs has never been studied. In this paper, we use an ensemble of global climate models and multiple thermal indices to robustly examine the combined effect of air temperature and relative humidity on COHs globally on an hourly basis. Our findings reveal that COHs show an increasing trend in the future and a strong latitudinal gradient increasing from high latitudes to the equator. Compared to COHs based on air temperature, the frequency of COHs based on perceived temperature is amplified by the combined effects of high temperature and humidity for both boreal and austral summers. To investigate the underlying mechanisms, we examine two different diurnal temperature ranges (DTRs), derived from air temperature and perceived temperature, for their corresponding types of COHs. Both DTRs are projected to increase in the future relative to the historical period from 1980 to 2004, but the DTR changes derived from perceived temperature are consistently larger than those derived from air temperature. Due to the nonlinearity in thermal indices, the perceived temperature in HDs and HNs rising faster than air temperature leads to a larger increase in perceived COHs. The COHs are further amplified by the increasing number of HNs and HDs that occur consecutively under wet conditions.

1 Introduction

Hot days (HDs) or hot nights (HNs) have adverse impacts on society and ecosystems (Braganza et al. 2004; Easterling et al. 1997; Vose et al. 2005; Zhou et al. 2004). Under climate warming, the increasingly sequential occurrence of HDs and HNs within 24 h further exacerbates adverse impacts on human health (Chen et al. 2019; Wang et al. 2020a, b; Wernberg et al. 2013). The consecutive occurrence of daytime and nighttime hot extremes (COHs) is widely used as a measure of the persistence of an extremely hot spell to explain spatial and temporal variations in excess mortality during heatwaves (Chen and Zhai 2017; Raymond et al. 2020; Wang et al. 2020a, b; Xu et al. 2019). Previous studies found that prolonged heat could strongly amplify health effects by inhibiting the recovery from the daytime heat and by exacerbating the impact through sleep deprivation (Chen et al. 2018; Ho et al. 2017; King et al. 2016; Meehl and Tebaldi 2004; Pal and Eltahir 2015). COHs are often measured using daily or hourly near-surface air temperature (AT) as a single indicator (Chen and Zhai 2017; Horton et al. 2016; Vaidyanathan et al. 2016; Wang et al. 2020a, b). However, the combined effect of high AT and high relative humidity (RH), which can lead to increased thermal stress on human body, has never been examined for COHs events. Neglecting such a combined effect could result in a substantial underestimation of heat-induced consequences (Mora et al. 2017; Willett et al. 2007; Willett and Sherwood 2012). Hence, it is worthwhile to investigate how COHs respond to the changing climate by taking into account the combination of AT and RH. In this study, we apply thermal indices to represent the combined effect of AT and RH and quantify the resulting equivalent temperatures perceived by humans. Furthermore, we examine the underlying diurnal relationship between AT and RH, which can further complicate the nighttime and daytime hot conditions. Generally, HNs occur under humid conditions, whereas HDs

✉ Shuo Wang
shuo.s.wang@polyu.edu.hk

1 School of Geography and Planning, Sun Yat-Sen University, Guangzhou, China

2 Department of Land Surveying and Geo-Informatics, The Hong Kong Polytechnic University, Hong Kong, China

3 Institute for Atmospheric and Climate Science, ETH Zurich, Zurich, Switzerland

occur under relatively dry conditions. The high RH enhances the greenhouse effect, reduces longwave radiation cooling and upholds nighttime temperature, while the low RH results in an enhancement of solar radiation heating the air near the surface to increase the daytime temperature (Chen and Lu 2014).

People living in different regions have different acclimation capacities to the change in temperature. Previous studies have not reached a consensus on the definition of thresholds used for different hot conditions. To address this issue, we use the 95th percentile of maximum or minimum (equivalent) temperatures in the historical period from 1980 to 2004. It helps indicate the hot condition and reflects on various implications for public health across different locations. For example, mean temperatures are generally low in the mid-latitude areas where the temperature above 28 °C would exceed the 95th percentile and thus cause thermal discomfort, whereas the same temperature would be nearly 5° below the 95th percentile at the low latitudes where 28 °C may be perceived as a comfortable temperature. Therefore, we define the (human-perceived) HDs as the hot days with maximum (human-perceived) temperatures above the 95th percentile of maximum (human-perceived) temperatures in the reference period. Contrarily, we define the (human-perceived) HNs as the hot nights with minimum (human-perceived) temperatures above the 95th percentile of minimum (human-perceived) temperatures in the reference period. Moreover, we use COHs to represent the consecutive occurrence of HDs and HNs on the same day. Similarly, we use the human-perceived COHs to represent the consecutive occurrence of human-perceived HDs and HNs within 24 h. To robustly assess the combined effect of air temperature and relative humidity on COHs, we conduct comparative analyses on the two different types of COHs and explore the underlying mechanisms.

2 Data and methods

An ensemble of global climate models (GCMs) and multiple thermal indices were used in this study. The hourly AT and RH were extracted from an ensemble of five GCM simulations (IPSL-CM5A-LR, GFDL-ESM2M, GFDL-ESM2G, FGOALS-g2, and MIROC-ESM described in Supplementary Table S1) to investigate their interactive relationships. The RH has a strong diurnal cycle opposite to the diurnal cycle of AT. Thus, combining daily maximum and minimum AT with daily mean RH would lead to a systematic bias. We evaluated the spatial patterns of AT and RH derived from hourly GCM outputs against the ERA5 reanalysis over 1980–2004 (Supplementary Figs. S1, S2). The model bias of GCMs for the historical period can systematically propagate into future projections. To minimize the effect of model biases, we investigated the changes in the extreme event that could be assessed by subtracting the historical simulation from the future projection. We focused on the high emission scenario RCP8.5 in which the CO_2 concentration is continuously increasing through 2100 and the aggressive mitigation scenario RCP2.6 that limits the warming to below 2 °C (Taylor et al. 2012).

We performed a comprehensive analysis of equivalent temperatures using an ensemble of thermal indices. Thermal indices have been widely used to quantify the perceived temperature that can cause thermal stresses to a person (Staiger et al. 2012). These equivalent temperatures have the same unit as AT and, therefore, can be analyzed consistently. Given recent climate change and various physiological constraints, it is unlikely that human physiology will necessarily evolve with higher heat tolerance (Hanna and Tait 2015; Mora et al. 2017; Sherwood et al. 2010). Hence, the body-related inputs were excluded from this study, and the perceived temperature was assessed only with atmospheric inputs (Bobb et al. 2014; Gasparrini et al. 2015; Lowe et al. 2011). Among all indices, HEI (Heat Index), HUM (Humidex), and AP (Apparent Temperature) have the advantages of high usability and being well-validated for measuring the perceived temperature globally (Buzan et al. 2015; Havenith and Fiala 2016; Roghanchi and Kocsis 2018; Wang and Zhu 2020; Zhu et al. 2019). The thermal indices, calculated on a seasonal (summer) basis, were adopted to robustly assess the heat stress. All outputs of the three indices are temperature equivalents in degree Celsius. HUM (Masterson 1979), HEI (Steadman 1979; Karl and Knight 1997), and AP (Steadman 1984) are defined as follows.

$$\mathrm{HUM} = \mathrm{AT} + 0.5555 \times \left(6.11 \times e^{5417.7530 \times \left(\frac{1}{273.16} - \frac{1}{273.15 - T_{dew}}\right)} - 10\right) \tag{1a}$$

$$T_{dew} = \frac{B \times \left[\ln\left(\frac{RH}{100}\right) + \frac{A \times AT}{B + AT}\right]}{A - \ln\left(\frac{RH}{100}\right) - \frac{A \times AT}{B + AT}} \tag{1b}$$

$$A = 17.625 \tag{1c}$$

$$B = 243.04 \tag{1d}$$

$$\begin{aligned} \mathrm{HEI} = {} & -8.7847 + 1.6114 \times \mathrm{AT} - 0.012308 \\ & \times \mathrm{AT}^2 + \mathrm{RH} \times (2.3385 - 0.14612 \times \mathrm{AT} \\ & + 2.2117 \times 10^{-3} \times \mathrm{AT}^2) + \mathrm{RH}^2 \\ & \times (-0.016425 + 7.2546 \times 10^{-4} \times \mathrm{AT} \\ & - 3.582 \times 10^{-6} \times \mathrm{AT}^2) \end{aligned} \tag{2}$$

$$AP = 1.04 \times AT + 2 \times e - 0.65 \times Wnd - 2.7 \tag{3}$$

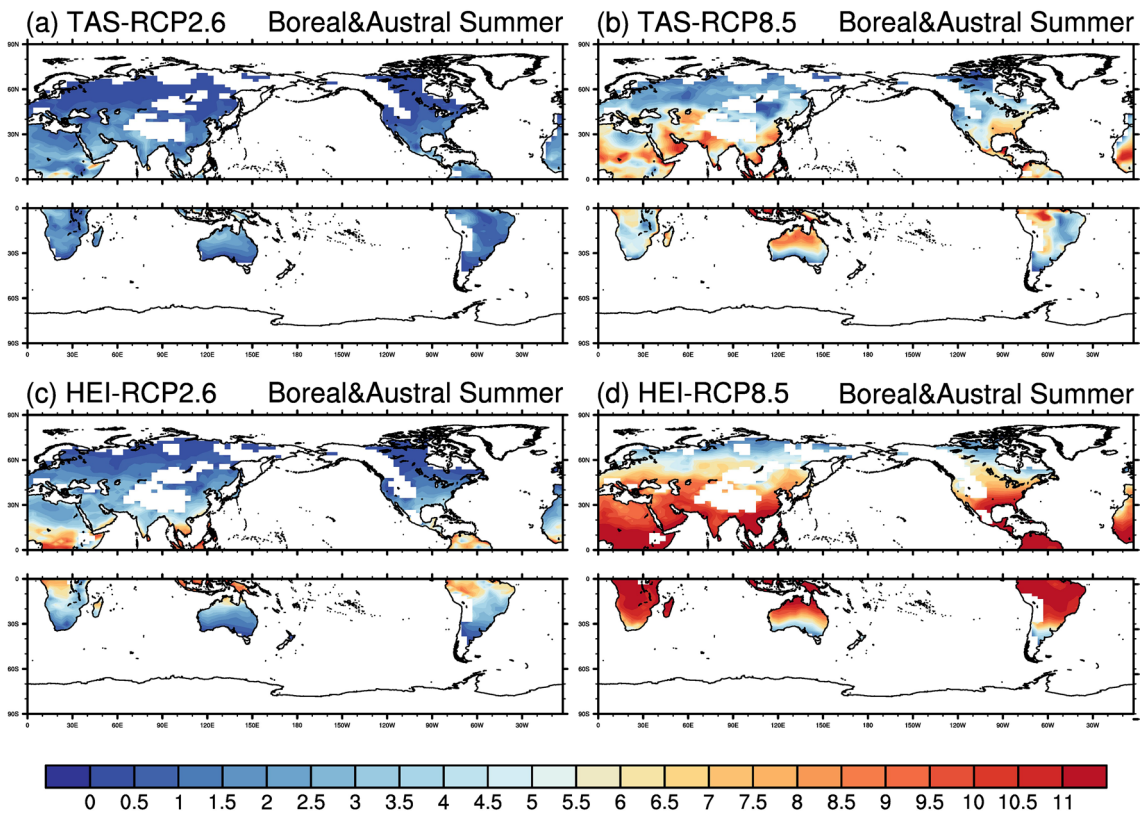

Fig. 1 The spatial pattern of the COH changes (days) derived from AT and the perceived COH changes (days) derived from HEI for 2076–2100 relative to 1980–2004. **a** Upper panel, the COH changes over the Northern Hemisphere (NH) under RCP2.6 for the boreal summer (JJA); Lower panel, the COH changes over the Southern Hemisphere (SH) under RCP2.6 for the austral summer (DJF). **b** Upper panel, the COH changes over NH under RCP8.5 for JJA; Lower panel, the COH changes for SH under RCP8.5 for DJF. **c** Upper panel, the perceived COH changes over NH under RCP2.6 for JJA; Lower panel, the perceived COH changes over SH under RCP2.6 for DJF. **d** Upper panel, the perceived COH changes over NH under RCP8.5 for JJA; Lower panel, the perceived COH changes over SH under RCP8.5 in DJF. For all maps, white areas indicate the missing values for air temperatures below 26 °C which is the valid temperature level for the HEI calculation

where *RH* is the hourly relative humidity (%), T_{dew} is the dew point temperature (°C), *Wnd* is the wind speed at 10 m of height (m/s), *e* is the simultaneous vapor pressure (hPa), and *AT* is the hourly maximum/minimum temperature (°C). Hourly human-perceived equivalent temperatures are calculated from the hourly AT and RH inputs. The maximum and minimum human-perceived temperatures can be derived from the hourly time series of equivalent temperatures. By applying the 95th percentile thresholds, the human-perceived HDs and HNs can be obtained. The valid temperature range of HEI for assessing the combined effect of AT and RH is over 21 °C. To keep the consistency in the comparison between the results derived from AT and thermal indices, HDs and HNs with their AT that are lower than 21 °C were excluded from the study.

Based on the outputs of derived HDs and HNs, we first examined the consecutive occurrence of HDs and HNs (COHs) for both historical and future periods. Then we calculated the change in COHs by subtracting the values of COHs in the historical period from the values in the future period (2076–2100). Second, we performed a similar calculation for the human-perceived COHs to assess their future changes relative to the reference period. Third, we compared the changes in the two different types of COHs and then identified the potential drivers. Fourth, we examined whether the DTR change contributed to the variation in COHs. Last, we compared the persistent heat and large-scale circulation anomalies associated with HDs and HNs under different humid conditions to understand the underlying mechanisms.

3 Results

Figure 1 presents the frequency changes in (perceived) COHs in the future relative to the reference period under RCP2.6 and RCP8.5. These frequencies are calculated from the number of days with both sub-daily maximum and

minimum (perceived) temperatures exceeding their corresponding thresholds for the boreal (JJA; June–July–August) and austral summers (DJF; December–January–February). Both COHs show positive changes for most parts of the world under both RCPs, but the magnitude of perceived COH change is greater than the COH change derived solely from AT. The combined effect of AT and RH largely amplifies the COH changes under both RCPs. The changes in both COHs demonstrate a strong latitudinal gradient increasing from high latitudes to the equator. The amplification of perceived COHs induced by the combined effect of AT and RH is strongest over the most humid and warm regions. For both seasons (boreal and austral summers), we find that tropical regions (for example, Western Africa, Eastern Africa, Amazon Basin, and Southeast Asia) will be exposed to the perceived COH for more than 5 days per year under RCP2.6 by the end of this century. The increased number of days is, as expected, higher under RCP8.5 (by a factor of 4 relative to the reference period) than the number under RCP2.6 (by a factor of 2). Results obtained based on the other two thermal indices (Supplementary Fig. S3) also exhibit a similar spatial pattern of the perceived COH with small variations in magnitudes. The different nonlinearities in thermal indices (Supplementary Fig. S4) have a relatively small effect on assessing the frequency changes in (perceived) COHs. The spatial pattern of changes in the perceived COH is consistent across all thermal indices, which increases our confidence in the robust assessment of heat stress and related extremes.

To facilitate further understanding of spatial characteristics of COH changes, we analyzed the regional changes in both COHs over 21 regions (Supplementary Fig. S5). The greatest regional increase in the perceived COH is projected over tropical regions such as Southeast Asia, Central America, Western Africa, Eastern Africa, and Amazon Basin in

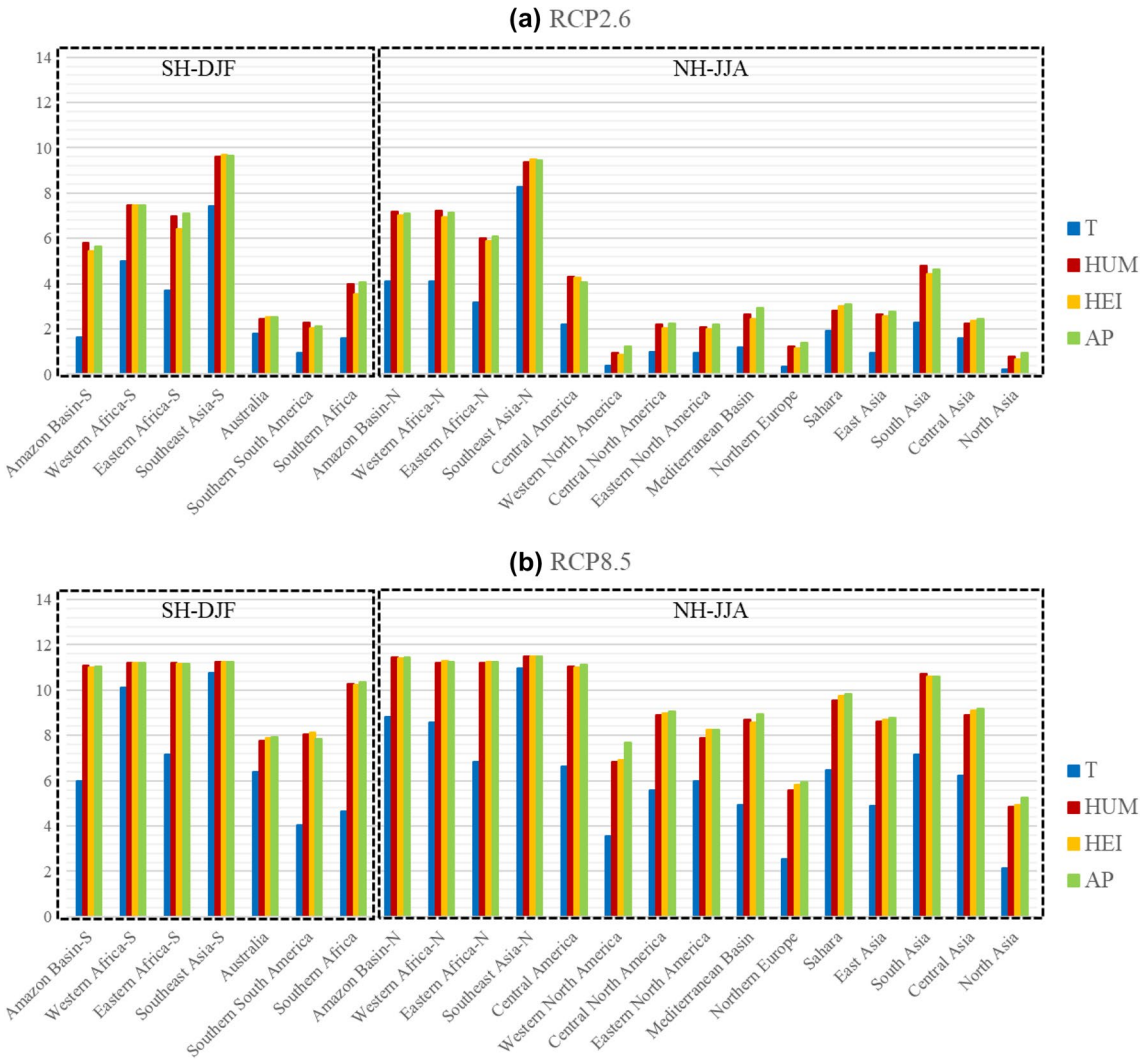

Fig. 2 Regional average of the COH changes (days) derived from AT and the perceived COH changes (days) using three thermal indices over 21 regions under RCP2.6 (**a**) and RCP8.5 (**b**) for boreal and austral summers

JJA or DJF (as shown in Fig. 2). It can be explained by that the tropics have a small seasonal cycle and relatively little year-to-year variability in AT. Thus, the same warming in low-latitude regions could lead to a much higher exceedance of the thresholds than in the mid- and high-latitude regions. Moreover, these regions have the year around high temperature and humidity, which already experience the frequent COHs derived from AT. These regions will have the greatest potential to amplify COHs by considering the combined effect of AT and RH. In addition to tropical regions, the regions with proximity to the ocean (East Asia, Eastern North America, Western North America, and the Middle East) are also experiencing the amplified COHs due to the abundant moisture supply from the ocean. The health-related risks of perceived COH may particularly increase in these coastal regions where the perceived daytime temperatures are cooler than tropical regions in the present-day climate. Residents living in these regions may be less physiologically acclimated (the body can get used to higher temperatures up to a level) and less behaviorally adapted to HDs and HNs. With the amplified COHs, outdoor workers in places such as agricultural and construction sites can no longer avoid the heat by shifting their work hours earlier or later in the day. Most large cities in the world are coastal cities or close to large bodies of water. People living in these cities are more likely to suffer from the daytime heat and have little relief at night than the residents living in other areas due to the urban heat island effect (Davy et al. 2017; Fischer and Knutti 2013; Fischer et al. 2012; Fischer and Schar 2010; Harrington et al. 2016; King et al. 2015).

To assess the sensitivity and the robustness of future projections to the choice of thermal indices, climate models, and emission scenarios, we examined the 10th to 90th percentile ranges of the projected COHs derived from five GCMs (Fig. 3), based on AT, HUM, HEI, and AP under two RCPs for both boreal and austral summers. Despite large uncertainties in the magnitude of future changes, all models consistently show that the overall changes in both types of COHs are substantially smaller under RCP2.6 than those under RCP8.5. The uncertainty in climate models used to derive both COHs is larger than the uncertainty in emission scenarios across all 21 regions. Nevertheless, all models agree on the spatial pattern, i.e., those tropics and coastal areas do show larger changes than other regions. Consequently, our study highlights that the insensitivity of changes in perceived COHs to thermal indices increases our confidence in the robust assessment of climate change impacts on COHs and their potential health-related effects. Since RH reaches its peak at night and drops to the bottom in the daytime, HNs would occur under more humid conditions than HDs. Intuitively, HNs would be amplified greater than HDs from the perspective of perceived temperature. Hence, the DTR derived from perceived temperatures would decrease accordingly. When we compute extremes without excluding temperatures that are lower than 21 °C, it is found that the daily mean DTR shows a negative change over most parts of continents (Supplementary Fig. S6). The finding coincides with previous studies revealing that the reduction in the daily mean DTR could lead to an increasing frequency of consecutive occurrence of daytime and nighttime hot conditions (Chen and Zhai 2017; Wang et al. 2020a, b). To investigate the mechanisms behind the amplification of COHs, we analyzed and compared the DTRs derived from two different types of COHs.

As shown in Fig. 4, DTRs for both COHs show increasing trends over continents for future JJA and DJF relative to the reference period. Changes in DTRs for perceived COHs based on HEI are similar to changes in DTRs for COHs based on AT in terms of spatial patterns, but the magnitudes of changes are larger for HEI than AT. The maximum temperatures of HDs rising faster than the minimum temperatures of HNs contributes to the increase in DTRs. As shown in Supplementary Fig. S7, more events are found above the thresholds in the plots for maximum temperatures than for minimum temperatures (with only considering temperatures over 21 °C). Due to the inherent nonlinearity, equal warming starting at higher temperatures leads to a greater increase of thermal index than those starting at lower temperatures (Supplementary Fig. S4). Since the daytime AT is higher than the nighttime AT, the uniform warming at a constant RH would lead to larger increases in perceived temperatures of HDs than of HNs. However, there is no latitudinal gradient in the spatial patterns of changes in both DTRs. As shown in Fig. 5, substantial changes in the perceived DTR are found over the tropical regions (i.e., Eastern and Western Africa, Southeast Asia), high-latitude areas (i.e., North Asia and Northern Europe), and mid-latitude regions (i.e., East Asia and North America). Dry regions, such as Sahara, Central Asia, and Mediterranean Basin, have relatively small changes in the perceived DTR because of their relatively low levels of RH. This is because the high or low nonlinearity of thermal indices can amplify the magnitudes of the perceived DTR changes to different extents (as shown in Fig. S4, per degree warming at constant RH, HUM, and AP projects the perceived temperature increases greater than HEI). Similar to the results derived from HEI, results from HUM and AP also exhibit an amplification in the perceived DTR relative to the DTR calculated from AT (Supplementary Fig. S8). But the perceived DTR changes derived from HEI are smaller than those derived from HUM and AP for all regions in terms of magnitude. Thus, we examined the 10th to 90th percentile ranges of GCMs for the projected DTR changes (Supplementary Fig. S9), based on AT, HUM, HEI, and AP under two RCPs, to explore the sensitivity to thermal indices, climate models, and emission scenarios. Results indicate that the DTR changes are more sensitive to the choice of

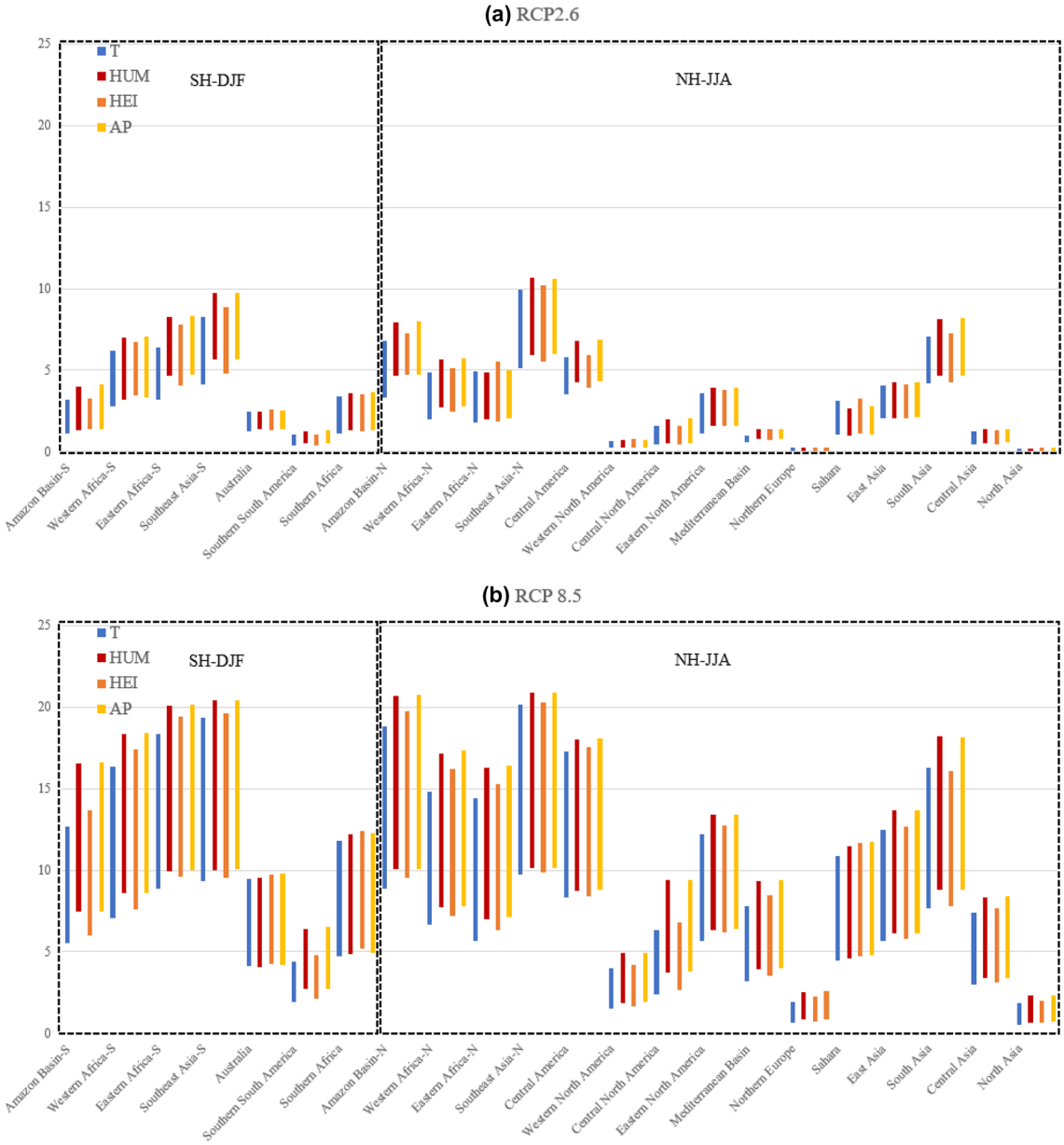

Fig. 3 The 10th to 90th percentile range of projected changes in the COH (days) derived from AT and the perceived COH (days) using three different thermal indices, based on model results obtained under RCP2.6 (**a**) and RCP8.5 (**b**)

thermal indices compared to model and scenario selections. Therefore, the amplification of COHs cannot be explained by a larger increase in perceived DTRs than DTRs based on AT because of the inconsistencies in latitudinal gradients and sensitivities to the selection of thermal indices. But the nonlinearity in thermal indices also exacerbates heat stress through the combined effect of high AT and RH. For a given level of warming, the perceived temperature increases at a faster rate than AT. In Fig. S7, considerably more events are found above thresholds in plots for thermal indices than for AT. Therefore, perceived temperatures above the thresholds occur for more days and nights, which further increases the frequency of COHs.

We further examined the atmospheric temperature and humid conditions in HDs and HNs for each COH event in order to identify the underlying drivers for the amplification of COHs. For the perceived COH, a large proportion of HNs, accounting for 86% of total events, occurs under wet conditions (RH > 60%). For the corresponding HDs, 54% of total events take place under humid conditions. The configuration of high temperature and humidity enhances their combined effect, thereby leading to the increase in COHs. To better understand the physical mechanisms behind the

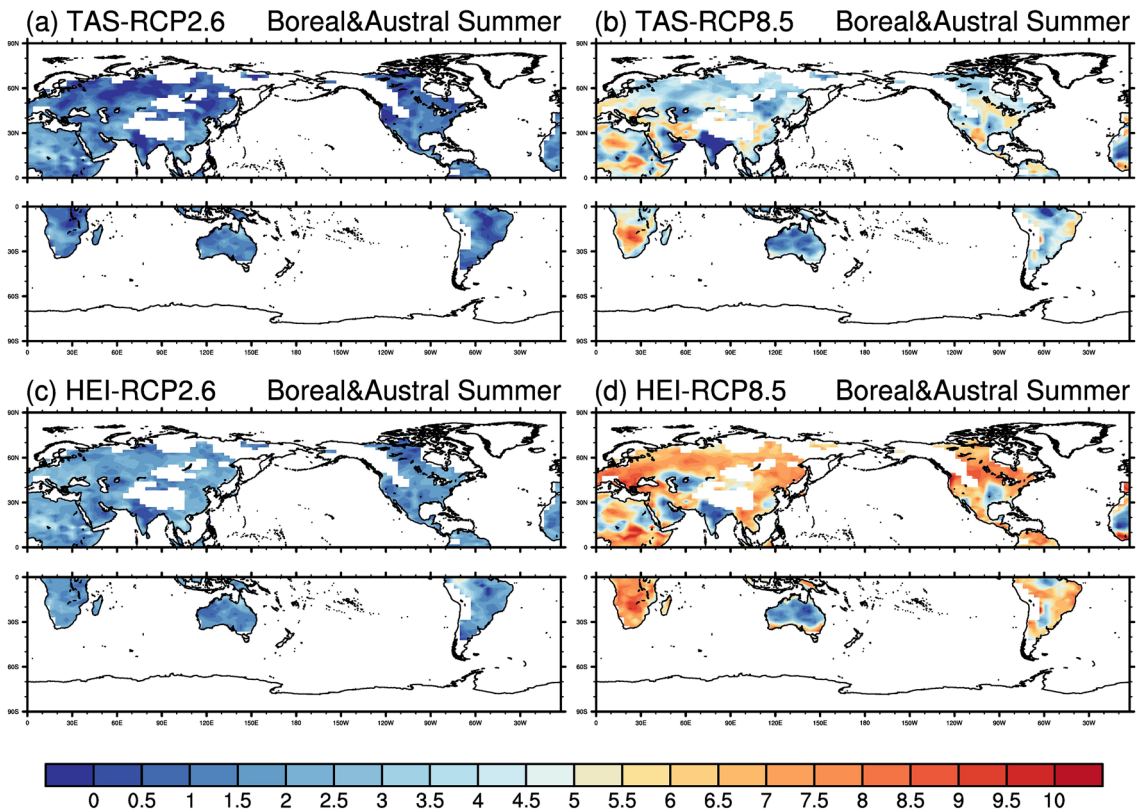

Fig. 4 Ensemble-mean changes in the DTR (°C) derived from AT and the perceived DTR (°C) based on HEI for 2076–2100 relative to 1980–2004. **a** Upper panel, the DTR changes over NH under RCP2.6 for JJA; Lower panel, the DTR changes over SH under RCP2.6 for DJF. **b** Upper panel, the DTR changes over NH under RCP8.5 for JJA; Lower panel, the DTR changes over SH under RCP8.5 for DJF. **c** Upper panel, the perceived DTR changes over NH under RCP2.6 for JJA; Lower panel, the perceived DTR changes over SH under RCP2.6 for DJF. **d** Upper panel, the perceived DTR changes over NH under RCP8.5 for JJA; Lower panel, the perceived DTR changes over SH under RCP8.5 for DJF

configuration of high AT and RH, we investigated the persistent heat (minimum AT > 25 °C) and the large-scale circulation anomaly from the preceding night of a COH event (Li et al. 2018a, 2018b; Ren et al. 2020; Zhao and Zhou 2019). As shown in Fig. 6, the minimum AT and 500-hPa velocity anomaly (e500) preceding a COH event are investigated to assess the contributions of these two factors to HDs and HNs consecutively occurring under different humidity conditions. For a COH with dry HD and wet HN, about half (49%) cases are preceded by a minimum AT over 25 °C. Up to 72% of overall cases are associated with positive e500s, which indicates an anomalous descent preceding the COH event. The adiabatic warming causes the dry air to move downward from the higher atmosphere layer and thus lower the humidity at the Earth's surface. For a COH with wet HD and wet HN, 70% of cases are preceded by a minimum AT over 25 °C, which indicates that the persistent heat greatly contributes to the configuration of high AT and high RH. The percentages of cases for positive and negative e500s are 46% and 54%, respectively. The COH with dry HD and dry HN as well as the COH with wet HD and dry HN are not investigated and plotted here due to the lack of statistical significance as a result of the small sample size. There is no strong correlation between the large-scale circulation anomaly and the COH with wet HD and wet HN. It is thus the persistence of high temperature that contributes to the consecutive occurrence of wet HNs and wet HDs.

4 Conclusions and discussions

In this paper, we examined the combined effect of AT and RH on the changes in COHs and carried out a comparative analysis of two different types of COHs derived from AT and perceived temperatures. The frequency of perceived COHs is amplified by the combined effects of high AT and RH under both RCPs for both boreal and austral summers. But both COHs demonstrate an increasing trend and a strong latitudinal gradient increasing from high latitudes to the equator. The greatest increase in the frequency of perceived COH is projected over tropical regions and some regions with proximity to the ocean due to the abundant moisture. These

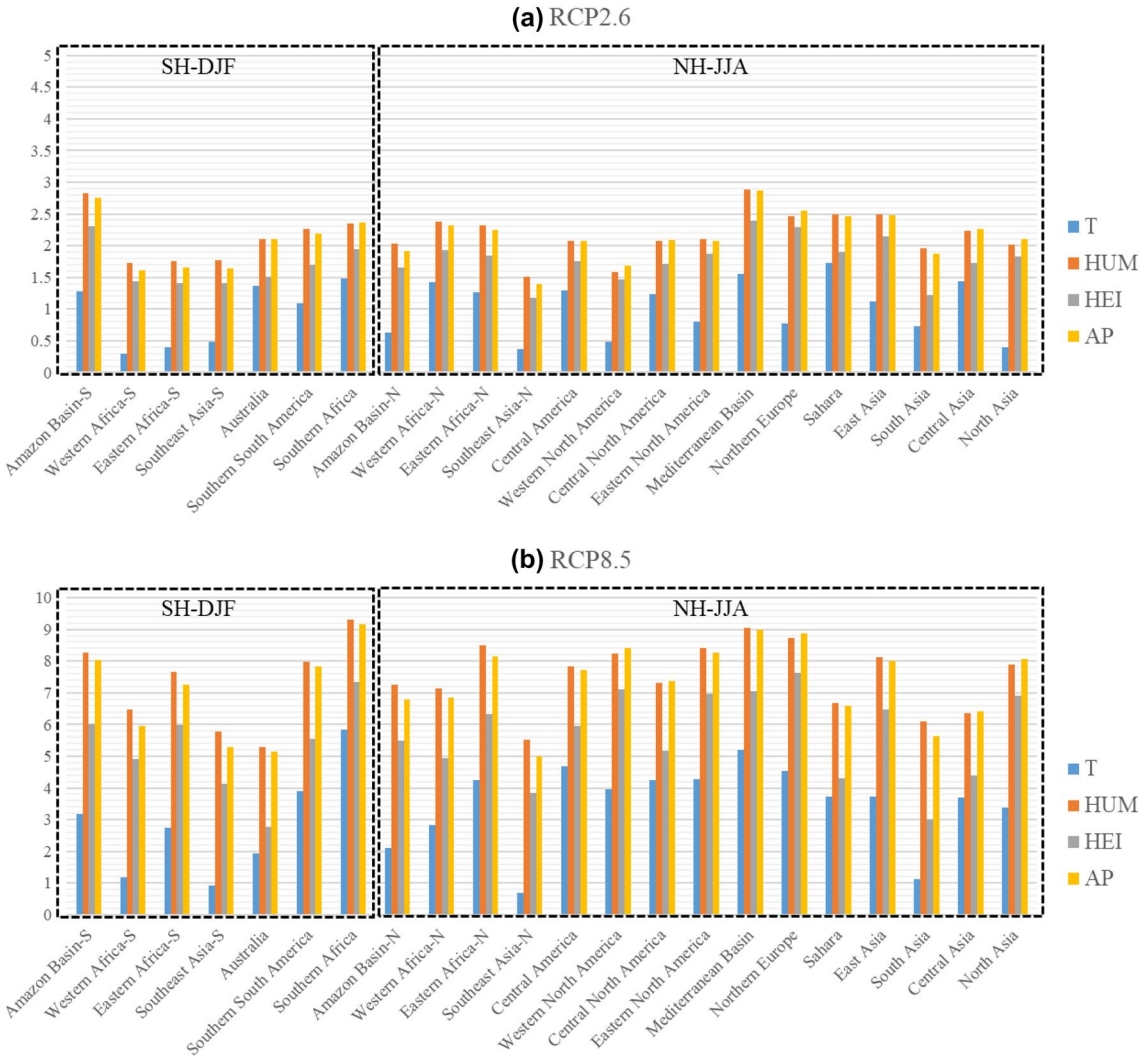

Fig. 5 Regional average of ensemble-mean changes in the DTR (°C) derived from AT and the perceived DTRs (°C) using three thermal indices over 21 regions (Amazon, Western Africa, Eastern Africa, and Southeast Asia are divided into two parts accordingly by the equator) under RCP2.6 (**a**) and RCP8.5 (**b**) for both boreal and austral summers (2076–2100 relative to 1980–2004)

coastal regions could have disastrous consequences because their temperatures are cooler than those over the tropics in the historical period. Residents living in these regions can be less physiologically acclimated and behaviorally adapted to the amplified COHs. In addition, we investigated the sensitivity of changes in perceived COHs to different sources of uncertainty. It is found that thermal indices have a much smaller influence on the changes in perceived COHs compared to models and emission scenarios. The insensitivity of changes in perceived COHs to the choice of thermal indices increases our confidence in the robust assessment of global warming impacts on heat stress through considering the combined effect of AT and RH.

To understand the mechanisms behind the amplification of COHs, we further analyzed the DTRs for two different types of COH events identified by AT and perceived temperatures. Our findings reveal that DTRs are projected to increase because some nighttime hot extremes with their temperature lower than 21 °C are excluded while considering the valid temperature range for computing the combined effect of AT and RH. However, no latitudinal gradient in DTR changes is found to coincide with the latitudinal gradient in COH changes. Moreover, DTR changes are sensitive to the choice of thermal indices. Therefore, the increases in COHs cannot be explained by the changes in their corresponding DTRs. Due to the nonlinearity in impact-relevant thermal indices, the perceived temperature increases at a faster rate than AT for a given level of warming. An increasing number of hot extremes takes place under wet conditions. The configuration of high temperature and humidity exacerbates the combined effect of AT and RH and further amplifies the frequency of COHs. To explore the underlying drivers of COHs changes, we further examined the persistent

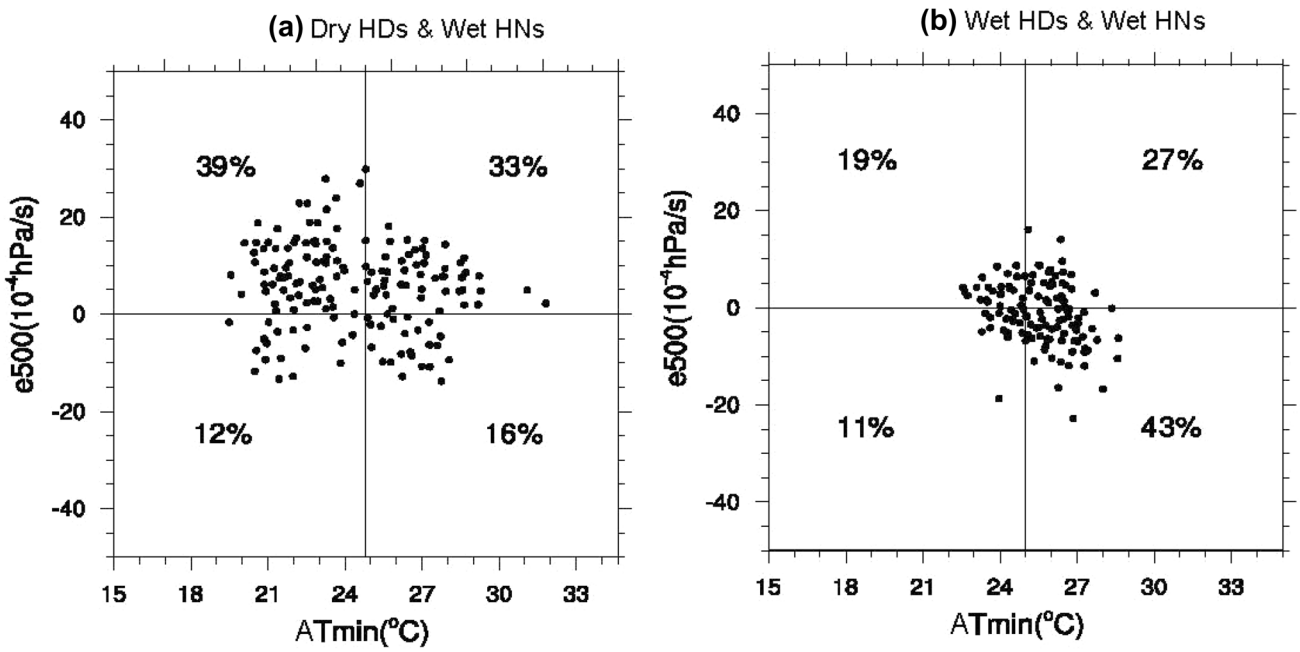

Fig. 6 Scatterplot of the minimum ATs (ATmin in plots; °C) and 500-hPa velocity anomalies (e500 in plots; 10^{-4} hPa/s) preceding dry HD and wet HN events (**a**), and wet HD and wet HN events (**b**)

heat and the large-scale circulation anomaly associated with HDs and HNs under different humidity conditions. We find that, in addition to the 500-hPa velocity anomaly, the persistence of high temperature (over 25 °C) of the preceding night contributes more to the consecutive occurrence of HNs and HDs under wet conditions. These increases in COHs are robust to the variation in the reanalysis dataset. However, differences between the reanalysis dataset and in-situ observations have not been systematically examined on an hourly basis due to data unavailability.

Supplementary Information The online version contains supplementary material available at https://doi.org/10.1007/s00382-021-06038-7.

Acknowledgements This research was supported by the National Natural Science Foundation of China (Grant no. 51809223) and the Hong Kong Research Grants Council Early Career Scheme (Grant no. 25222319). Readers can find the data that support or underlie the conclusions presented in the Mendeley Data (http://dx.doi.org/10.17632/7jfn3xxvpw.1). CMIP5 data used in this paper are freely available at https://esgf-node.llnl.gov/projects/cmip5/. We acknowledge and thank the climate modeling groups (listed in Supplementary Table S1) in the World Climate Research Programme's Working Group on Coupled Modelling (which is responsible for CMIP5) for generating their model outputs and making them available. The authors declare no competing financial interests.

Author contributions Jinxin Zhu and Shuo Wang conceived the study and conducted the analysis. Jinxin Zhu and Shuo Wang contributed equally to the writing and discussion of ideas. Erich M. Fischer provided comments and suggestions for improving the quality of this study.

References

Bobb JF, Peng RD, Bell ML, Dominici F (2014) Heat-related mortality and adaptation to heat in the United States. Environ Health Perspect 122(8):811–816. https://doi.org/10.1289/ehp.1307392

Braganza K, Karoly DJ, Arblaster JM (2004) Diurnal temperature range as an index of global climate change during the twentieth century. Geophys Res Lett. https://doi.org/10.1029/2004gl019998

Buzan JR, Oleson K, Huber M (2015) Implementation and comparison of a suite of heat stress metrics within the Community Land Model version 4.5. Geosci Model Dev 8(2):151–170. https://doi.org/10.5194/gmd-8-151-2015

Chen RD, Lu RY (2014) Dry tropical nights and wet extreme heat in Beijing: atypical configurations between high temperature and humidity. Mon Weather Rev 142(5):1792–1802

Chen Y, Zhai P (2017) Revisiting summertime hot extremes in China during 1961–2015: overlooked compound extremes and significant changes. Geophys Res Lett 44:5096–5103. https://doi.org/10.1002/2016GL072281

Chen Y, Zhai P, Zhou B (2018) Detectable impacts of the past half-degree global warming on summertime hot extremes in China. Geophys Res Lett 45:7130–7139. https://doi.org/10.1029/2018GL079216

Chen Y, Zhou B, Zhai P, Moufouma-Okia W (2019) Half-a-degree matters for reducing and delaying global land exposure to combined daytime-nighttime hot extremes. Earth's Future 7:953–966. https://doi.org/10.1029/2019EF001202

Davy R, Esau I, Chernokulsky A, Outten S, Zilitinkevich S (2017) Diurnal asymmetry to the observed global warming. Int J Climatol 37(1):79–93. https://doi.org/10.1002/joc.4688

Easterling DR et al (1997) Maximum and minimum temperature trends for the globe. Science 277(5324):364–367. https://doi.org/10.1126/science.277.5324.364

Fischer EM, Knutti R (2013) Robust projections of combined humidity and temperature extremes. Nat Clim Chang 3(2):126–130. https://doi.org/10.1038/Nclimate1682

Fischer EM, Schar C (2010) Consistent geographical patterns of changes in high-impact European heatwaves. Nat Geosci 3(6):398–403. https://doi.org/10.1038/Ngeo866

Fischer EM, Oleson KW, Lawrence DM (2012) Contrasting urban and rural heat stress responses to climate change. Geophys Res Lett. https://doi.org/10.1029/2011gl050576

Gasparrini A et al (2015) Temporal variation in heat-mortality associations: a multicountry study. Environ Health Perspect 123(11):1200–1207. https://doi.org/10.1289/ehp.1409070

Hanna EG, Tait PW (2015) Limitations to thermoregulation and acclimatization challenge human adaptation to global warming. Int J Environ Res Public Health 12(7):8034–8074. https://doi.org/10.3390/ijerph120708034

Harrington LJ, Frame DJ, Fischer EM, Hawkins E, Joshi M, Jones CD (2016) Poorest countries experience earlier anthropogenic emergence of daily temperature extremes. Environ Res Lett 11:055007. https://doi.org/10.1088/1748-9326/11/5/055007

Havenith G, Fiala D (2016) Thermal indices and thermophysiological modeling for heat stress. Compr Physiol 6(1):255–302. https://doi.org/10.1002/cphy.c140051

Ho HC, Lau KL, Ren C, Ng E (2017) Characterizing prolonged heat effects on mortality in a sub-tropical high-density city, Hong Kong. Int J Biometeorol 61(9):1–10

Horton RM, Mankin JS, Lesk C, Coffel E, Raymond C (2016) A review of recent advances in research on extreme heat events. Curr Clim Change Rep 2(4):242–259

Karl TR, Knight RW (1997) The 1995 Chicago heat wave: how likely is a recurrence? Bull Am Meteorol Soc 78(6):1107–1119. https://doi.org/10.1175/1520-0477(1997)078%3c1107:Tchwhl%3e2.0.Co;2

King AD, Donat MG, Fischer EM, Hawkins E, Alexander LV, Karoly DJ, Dittus AJ, Lewis SC, Perkins SE (2015) The timing of anthropogenic emergence in simulated climate extremes. Environ Res Lett 10:094015. https://doi.org/10.1088/1748-9326/10/9/094015

King AD, Black MT, Min S-K, Fischer EM, Mitchell DM, Harrington LJ, Perkins-Kirkpatrick SE (2016) Emergence of heat extremes attributable to anthropogenic influences. Geophys Res Lett 43:3438–3443. https://doi.org/10.1002/2015GL067448

Li D, Zhou T, Zou L, Zhang W, Zhang L (2018a) Extreme high-temperature events over East Asia in 1.5°C and 2°C warmer futures: analysis of NCAR CESM low-warming experiments. Geophys Res Lett 45(3):1541–1550. https://doi.org/10.1002/2017GL076753

Li D, Zou L, Zhou T (2018b) Regional air–sea coupled model simulation for two types of extreme heat in North China. Clim Dyn 50(5):2107–2120. https://doi.org/10.1007/s00382-017-3738-2

Lowe D, Ebi KL, Forsberg B (2011) Heatwave early warning systems and adaptation advice to reduce human health consequences of heatwaves. Int J Environ Res Public Health 8(12):4623–4648. https://doi.org/10.3390/ijerph8124623

Masterson JRFA (1979) Humidex, a method of quantifying human discomfort due to excessive heat and humidity. Environment Canada (Atmospheric Environment Service), Downsview, Ontario

Meehl GA, Tebaldi C (2004) More intense, more frequent, and longer lasting heat waves in the 21st century. Science 305(5686):994–997. https://doi.org/10.1126/science.1098704

Mora C et al (2017) Global risk of deadly heat. Nat Clim Chang 7(7):501–506. https://doi.org/10.1038/Nclimate3322

Pal JS, Eltahir EAB (2015) Future temperature in southwest Asia projected to exceed a threshold for human adaptability. Natu Clim Change 6(2):197–200

Raymond C, Matthews T, Horton RM (2020) The emergence of heat and humidity too severe for human tolerance. Sci Adv 6(19):eaaw1838. https://doi.org/10.1126/sciadv.aaw1838

Ren L, Zhou T, Zhang W (2020) Attribution of the record-breaking heat event over Northeast Asia in summer 2018: the role of circulation. Environ Res Lett 15(5):054018. https://doi.org/10.1088/1748-9326/ab8032

Roghanchi P, Kocsis KC (2018) Challenges in selecting an appropriate heat stress index to protect workers in hot and humid underground mines. Saf Health Work 9(1):10–16. https://doi.org/10.1016/j.shaw.2017.04.002

Sherwood SC, Ingram W, Tsushima Y, Satoh M, Roberts M, Vidale PL, O'Gorman PA (2010) Relative humidity changes in a warmer climate. J Gerontol Ser A Biol Med Sci. https://doi.org/10.1029/2009jd012585

Staiger H, Laschewski G, Grätz A (2012) The perceived temperature - a versatile index for the assessment of the human thermal environment. Part a: Scientific Basics. Int J Biometeorol 56(1):165–176. https://doi.org/10.1007/s00484-011-0409-6

Steadman R G (1979) Assessment of sultriness. 1. Temperature-humidity index based on human physiology and clothing science. J Appl Meteorol 18(7):861–873. https://doi.org/10.1175/1520-0450(1979)018<0861:Taospi>2.0.Co;2

Steadman RG (1984) A universal scale of apparent temperature. J Clim Appl Meteorol 23(12):1674–1687. https://doi.org/10.1175/1520-0450(1984)023%3c1674:AUSOAT%3e2.0.CO;2

Taylor KE, Stouffer RJ, Meehl GA (2012) An overview of CMIP5 and the experiment design. Bull Am Meteorol Soc 93(4):485–498. https://doi.org/10.1175/Bams-D-11-00094.1

Vaidyanathan A, Kegler SR, Saha SS, Mulholland JA (2016) A statistical framework to evaluate extreme weather definitions from a health perspective: a demonstration based on extreme heat events. Bull Am Meteorol Soc 97(10):1817–1830

Vose RS, Easterling DR, Gleason B (2005) Maximum and minimum temperature trends for the globe: an update through 2004. Geophys Res Lett. https://doi.org/10.1029/2005gl024379

Wang S, Zhu JX (2020) Amplified or exaggerated changes in perceived temperature extremes under global warming. Clim Dyn 54(1–2):117–127

Wang J, Feng J, Yan Z, Chen Y (2020a) Future risks of unprecedented compound heat waves over three vast urban agglomerations in China. Earth's Future 8:e2020EF001716. https://doi.org/10.1029/2020EF001716

Wang J, Chen Y, Tett SFB, Yan Z, Zhai P, Feng J, Xia J (2020b) Anthropogenically-driven increases in the risks of summertime compound hot extremes. Nat Commun 11(1):528. https://doi.org/10.1038/s41467-019-14233-8

Wernberg T, Smale DA, Tuya F, Thomsen MS, Langlois TJ, de Bettignies T, Bennett S, Rousseaux CS (2013) An extreme climatic event alters marine ecosystem structure in a global biodiversity hotspot. Nat Clim Chang 3(1):78–82

Willett KM, Sherwood S (2012) Exceedance of heat index thresholds for 15 regions under a warming climate using the wet-bulb globe temperature. Int J Climatol 32(2):161–177. https://doi.org/10.1002/joc.2257

Willett KM, Gillett NP, Jones PD, Thorne PW (2007) Attribution of observed surface humidity changes to human influence. Nature 449(7163):710-U716. https://doi.org/10.1038/nature06207

Xu L, Wang A, Wang D, Wang H (2019) Hot spots of climate extremes in the future. J Geophys Res Atmosp 124:3035–3049. https://doi.org/10.1029/2018JD029980

Zhao S, Zhou T (2019) Are the observed changes in heat extremes associated with a half-degree warming increment analogues for future projections? Earth's Future 7(8):978–992. https://doi.org/10.1029/2019EF001237

Zhou LM, Dickinson RE, Tian YH, Fang JY, Li QX, Kaufmann RK, Tucker CJ, Myneni RB (2004) Evidence for a significant urbanization effect on climate in China. Proc Natl Acad Sci USA 101(26):9540–9544. https://doi.org/10.1073/pnas.0400357101

Zhu J, Wang S, Huang G (2019) Assessing climate change impacts on human-perceived temperature extremes and underlying uncertainties. J Gerontol Ser A Biol Med Sci 124(7):3800–3821. https://doi.org/10.1029/2018jd029444